On the Dynamics of the Plasma Entry and Guiding in a Straight Magnetized Filter of a Pulsed Vacuum Arc

Leandro Giuliani, Fernando Minotti, Diana Grondona, and Héctor Kelly

***Abstract*—In this paper, a study of the plasma jet generated in a pulsed copper vacuum arc along a straight magnetized filter is presented. The ion saturation current and the plasma potential at different radial and axial positions and magnetic field intensities were measured using electrostatic probes. A theoretical model was developed to understand the dynamics of the plasma entry and guiding in the filter. This model takes into account magnetic field variations and Gaussian ion radial profiles. An analysis of the experimental results with the theoretical model shows that, in our device, as the magnetic field intensity increases along the filter, the plasma motion evolves from a radial compression with a low rotational velocity at the filter entrance to a rotating jet guided along the duct.**

***Index Terms*—Magnetic field, plasma jet, vacuum arc.**

I. Introduction

IN VACUUM arc discharges, a jet of plasma with energetic ions is spread out from the cathode [1]. Also, melted cathode material is emitted in the form of microdroplets. These microdroplets are undesired for some coating applications, because their presence increases the porosity and roughness of the coating, affecting the films properties. Up to now, the widely used system for removing microdroplets is magnetic filtering. This process consists of a magnetic field generated by a solenoid wound around a tube. The plasma flux is guided through the tube by the magnetic field, whereas the massive microdroplets stick on or bounce from the walls because they travel in almost straight lines. The tube can be a straight tube (rectilinear filter) or a curved one. The main drawback of these filters is the relatively high ion losses along the filter, thus resulting in a marked reduction of the deposition rate. The main ion losses occur at the filter entrance. For this reason, it is important to study the plasma transport to optimize the filtering system. Many experimental and theoretical works have been performed in this direction [2]–[5].

In a previous work [6], we presented experimental results and a very simplified theoretical model for the plasma transport in a rectilinear magnetic filter produced in a pulsed vacuum arc. The radial profile of the floating plasma potential and the ion saturation current were measured using electrostatic probes along the inner region of the filter, where the magnetic field intensity remains almost constant. The plasma rotation due to the presence of an axial magnetic field was particularly analyzed, using a hydrodynamic model that assumed a constant magnetic field value.

Following this line, in this paper, measurements with electrostatics probes have been made at the filter entrance. In this region, contrary to what happens in the central region of the filter, the field intensity changes considerably. Therefore, the previously developed theoretical model has been extended to include a magnetic field variation and more realistic ion radial profiles. An analysis of the experimental results with the theoretical prediction allowed us to understand the behavior of the plasma flux along the filter. We found that, in our device, as the magnetic field intensity increases along the filter, the plasma motion evolves from a radial compression with a low rotational velocity at the filter entrance to a rotating jet guided along the duct.

II. Experimental Setup

A schematic drawing of the experimental apparatus is shown in Fig. 1. The arc was pulsed for $\sim$35 ms, with an arc peak current (I_{A}) of (450 $\pm$ 20) A and an interelectrode voltage (V_{AC}) of (45 $\pm$ 5) V. The arc was produced by discharging an electrolytic capacitor bank with $C = 0.075$ F, connected to a series inductor-resistor $(L = 2$ mH, $R = 0.33\ \Omega)$, which critically damped the discharge [7]. The charging voltage was 260 V and the arc was ignited with a mechanically controlled tungsten trigger rod. The vacuum chamber was a stainless steel cylinder 25 cm long with a 10 cm (inner) diameter. The chamber pressure was maintained at a base pressure $< 10^2$ Pa during the whole arc discharge with an oil diffusion pump.

A grounded cathode (5 cm in length and 1 cm in diameter) was located in front of an annular anode with an aperture of 5 cm and a thickness of 2 cm. A grid was mounted on the cathode-facing side of the anode and kept at the same anode potential. The distance between the cathode frontal surface and the closest plane of the anode (grid position) was 1 cm. The lateral surface of the cathode was covered with a Pyrex insulator to ensure that the ion emission was through the cathode front surface.

At the end of the anode, separated by a 1-cm insulating ring, was placed the entrance of the magnetized duct at 3 cm from the cathode frontal surface. The magnetic field was established by an external coil wrapped around a stainless steel tube (22 cm long, 5 cm inner diameter). The coil was fed with dc current from an independent power source. The magnetic

Manuscript received April 13, 2007; revised June 26, 2007. This work was supported by Grants from the Buenos Aires University (X 111 and X 106), and the CONICET (PIP 5378).

The authors are with the Instituto de Física del Plasma (CONICET)—Departamento de Física, Facultad de Ciencias Exactas y Naturales, Universidad de Buenos Aires, 1428 Buenos Aires, Argentina (e-mail: leandro@tinfip.lfp.uba.ar).

Digital Object Identifier 10.1109/TPS.2007.910213

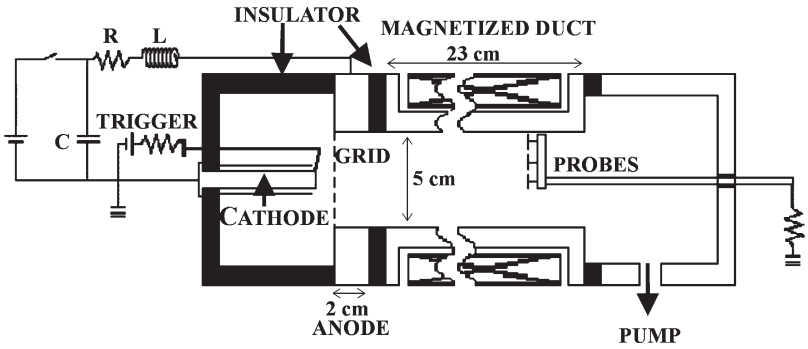

Fig. 1. Schematic drawing in scale of the experimental apparatus.

field strength was measured with a calibrated Hall probe. The investigated magnetic field values were those corresponding to coil currents of 42 and 80 A. The filter was also biased with another independent power source that could withstand bias currents of up to 50 A. In practice, since the plasma floating potential $(V_{\rm pf})$ in our case was higher than 30 V (see next section), the filter was biased at a nominal voltage of 80 V (with a resulting actual bias voltage that depends on the current collected by the filter). To insulate the duct from the arc discharge (thus avoiding the electron collection from the main arc discharge), a thin glass tube 4 cm long and with an outer diameter practically coincident with the duct inner diameter was glued to the insulating piece that coupled the anode and the duct. In this way, the duct acted as an insulator for the first 4 cm of its length.

Three circular plane copper probes (0.6 cm diameter) located at different radial positions in the tube were employed to register the plasma floating potential and the ion saturation current $(I_{\rm i}^{\rm p})$ as functions of the axial position along the tube [(d), measured from the cathode frontal surface] and the magnetic field intensity. One of the probes (probe 1) was located on the symmetry axis of the duct, while the other two (probes 2 and 3) were located at radial positions (r) of 1 and 2 cm from the duct axis (measured from the center of the coils), respectively. Taking into account the relatively high plasma potential (see next section), for the measurement of the ion saturation current, the probes were simply biased to ground through a small resistance to ensure that the probe voltage was well below $V_{\rm pf}$ during the discharge. The electrical signals were registered using a four-channel digitizing oscilloscope (500 MS $\cdot$ s^1 sampling rate, 100 MHz analogical bandwidth).

III. Results

Fig. 2 presents the magnetic field profiles (B_d) measured at the filter axis when the coil was carrying currents of 42 and 80 A. It can be seen that the magnetic field intensity varies considerably at the filter entrance and reaches its maximum value at the duct center. In this paper, the magnetic field intensity (B) was characterized with the value measured at the duct center ($r = 0$ cm and $d = 15$ cm), with values of 21.7 and 41.3 mT for the previously quoted coil currents.

The presence of the grid neither perturbed the interelectrode voltage nor the arc current, giving the same results than in previous works performed with the same equipment but without the

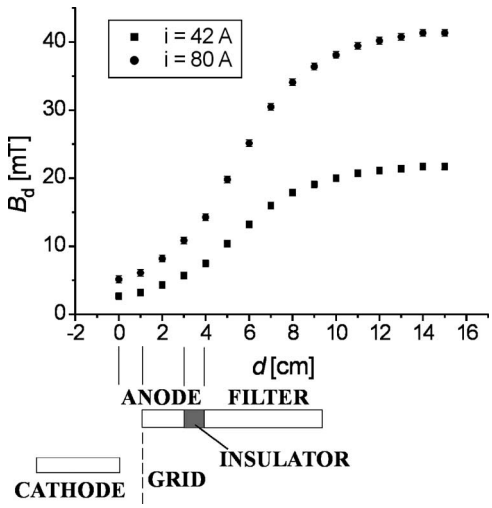

Fig. 2. Magnetic field profiles measured at the filter axis corresponding to two different coil currents. The discharge geometry is depicted at the bottom of the figure.

grid [6]. However, the grid did modify the ion current and the plasma potential but allowed the approximation of the probes to the cathode to perform measurements at the filter entrance. Because the magnetic field at the cathode position is small (below 5 mT), $V_{\rm AC}$ and $I_{\rm A}$ were both independent of B within experimental uncertainties, reaching values of (45 $\pm$ 5) V and (450 $\pm$ 20) A, respectively.

In Fig. 3, typical signals of $V_{\rm pf}$ and $I_{\rm i}^{\rm p}$ obtained with the three probes corresponding to $d = 10.5$ cm and $B = 21.7$ mT are presented. It can be seen that both quantities present a maximum at t $\sim$ 10 ms, corresponding with the peak in $I_{\rm A}$. To establish correlations between the different measured quantities, in what follows, we will use these peak values of $V_{\rm pf}$ and $I_{\rm i}^{\rm p}$ as representative of these quantities, without any distinction in the symbols. Since vacuum arcs are known to show marked fluctuations, each point in the graphs to be presented below will correspond to the average of five consecutive shots performed under the same operating conditions.

Fig. 4 shows the measured axial profiles of $V_{\rm pf}$ at three different radial probe positions ($V_{\rm pf}^1$, $V_{\rm pf}^2$, and $V_{\rm pf}^3$, corresponding to probes 1, 2, and 3, respectively), for the two investigated B values (21.7 and 41.3 mT). It can be seen that the three probes located at the same axial position present voltage differences which indicate the presence of a radial electric field $(E_{\rm r})$. These differences are increased as the probes are

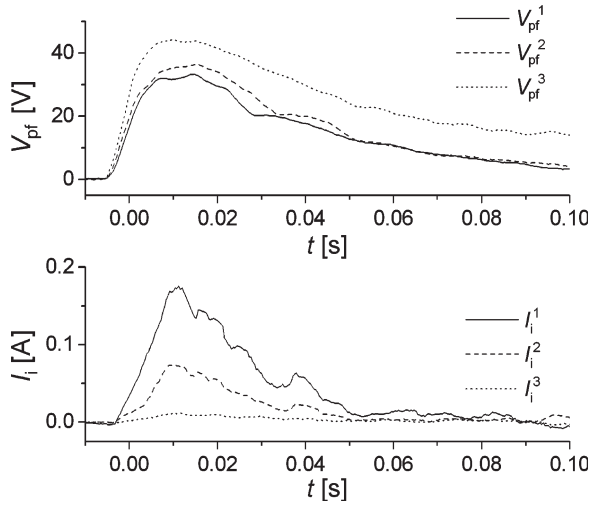

Fig. 3. (Top) Typical waveforms of the probes floating potential, and (bottom) the collected ion current corresponding to $d = 10.5$ cm and $B = 21.7$ mT.

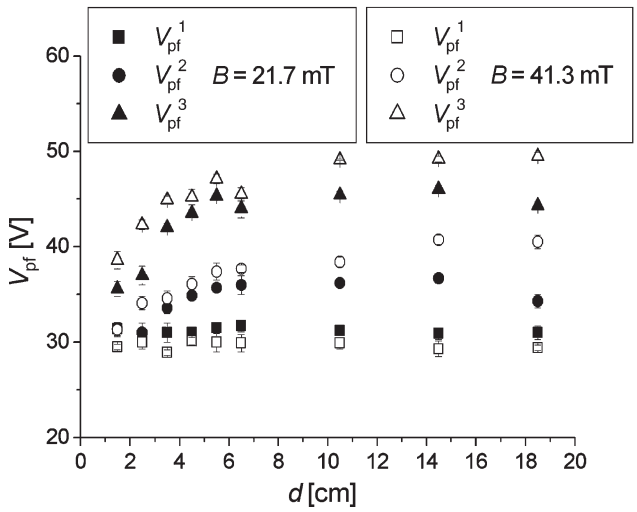

Fig. 4. Axial profiles of the plasma floating potential corresponding to the three radial positions ($V_{\rm pf}^1$, $V_{\rm pf}^2$, and $V_{\rm pf}^3$), for the two investigated values of B (21.7 and 41.3 mT).

moved away from the cathode, finally reaching a practically constant value at $d \sim 10$ cm. The described behavior is more pronounced for the largest B value. The floating voltages can be converted easily into plasma voltage $(V_{\rm p})$ values. This is so because the magnetic field is almost perpendicular to the probe's surface, and so the classical Langmuir probe's theory is valid, [8] corrected by Lam's work [9] to take into account ions of arbitrary kinetic energy. Hence, $V_{\rm p} = V_{\rm pf} + T_{\rm e}/e \ln\{[4m_{\rm i}/(\pi Z_{\rm i} m_{\rm e})]^{1/2}[1 + K_{\rm i}/(Z_{\rm i}T_{\rm e})]^{-12}\}$, where $T_{\rm e}$ is the electron temperature in energy units, $m_{\rm i}$ and $m_{\rm e}$ are the ion and electron masses, respectively, $K_{\rm i}$ is the ion kinetic energy and $Z_{\rm i}$ the average charge of the ion. Besides, since elastic and inelastic collisions are infrequent, the electron temperature $T_{\rm e}$ can be considered as a constant, and the same happens with $K_{\rm i}$, as is shown below. In this way, $V_{\rm p}$ and $V_{\rm pf}$ differ in an additive constant, so that the electric field can be determined using $V_{\rm pf}$ instead of $V_{\rm p}$. The electron temperature was determined from the slope of the electron current branch of the current–voltage characteristic of probe 1. To avoid misunderstandings in the interpretation of the electron branch of the probe characteristic due to the presence of the magnetic field, for the determination of $T_{\rm e}$, the case $B = 0$ and floating filter was selected, resulting in $T_{\rm e} = (2.0 \pm 0.4)$ eV.

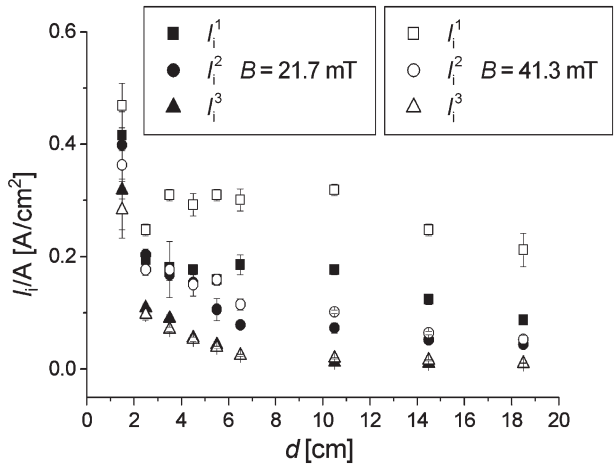

Fig. 5. Ion current to the probes ($I_{\rm i}^1$, $I_{\rm i}^2$, and $I_{\rm i}^3$, normalized to the probe areas) as functions of d for $B = 21.7$ mT and $B = 41.3$ mT.

In Fig. 5, the ion current to the probes as functions of d are presented for the two investigated B values. This figure shows that the ion current to the probes decreased markedly in the first 3 cm, corresponding to the anode region, whereas there was little change in the currents after this point, which is the entrance of the magnetic filter. It can be seen that the current distribution along the tube is much more concentrated at the duct center for large B values.

IV. Plasma Model

We used a simple model to describe the plasma entering the magnetic filter. The model is similar to that used in [6] with the addition of a nonuniform magnetic field and an extension to more realistic radial profiles of density and current. A time-independent plasma jet is considered, with azimuthal symmetry about the filter axis, representing the ions and electrons leaving the main discharge and entering the filter. The model equations are considered time independent because the ion transit time along the filter is very small (a few microseconds) compared to the discharge duration (a few tens of milliseconds). It is important to mention that the model is intended to describe the plasma that have effectively entered the filter and concentrates around the filter axis, forced by the radial electric field generated by the charge separation between the magnetized electrons and the nonmagnetized ions. Taking into account the described behavior of the ion current to the probes for $d \geq 3$ cm (see Fig. 5), plasma losses to the filter wall are neglected. The idea is to treat with some detail the ion dynamics, neglecting in their fluid equations the collisions with electrons, and the ion viscosity (these approximations were discussed in [6]). No equations are considered for the electrons; its only effect being the electric field they contribute to generate. It will be shown that, based on the assumptions made for the ion dynamics, the radial component of this electric field results a linear function

of the distance to the filter axis, with axial position dependent coefficients to be determined experimentally.

The charge conservation equation for the ion current density $\boldsymbol{j}$, in cylindrical coordinates, is, for the assumed symmetry

$$\frac{1}{r}\frac{\partial}{\partial r}(rj_r)+\frac{\partial j_z}{\partial z}=0. \tag{1}$$

The axial ion current density j_z is assumed to be distributed in the cross section of the plasma jet, according to a Gaussian profile given by [6]

$$j_z(r,z)=\frac{I_\mathrm{i}}{\pi R^2(z)}\exp\left[-r^2/R^2(z)\right] \tag{2}$$

so that $R(z)$ determines the ion current profile at each $z=$ const section of the jet. From (1) and (2), one obtains

$$j_r(r,z)=\frac{I_\mathrm{i}R'(z)}{\pi R(z)r}\left[2\left(1-\exp\left[-r^2/R^2(z)\right]\right)-r^2/R^2(z)\right]. \tag{3}$$

In this expression, $R'=dR/dz$, and I_i is the total ion current entering the filter (a small fraction of the arc current I_A). The positive z-direction is taken as that going from the cathode to the filter, that is, the direction in which the jet ions move, so that $I_\mathrm{i}>0$.

Since in our situation the I_A value is relatively large (450 A), the ions are ejected from several spots moving fast on the cathode surface. As the ions are ejected at small angles normal to the cathode surface [1], on the time average, it can be considered that the ion jet is emitted evenly distributed on the whole frontal cathode surface, with an approximately uniform axial ion velocity (u_Z) in each cross section of the jet, and with a relatively small radial velocity $(u_r)(u_r<0.2u_z)$, for emission angles smaller than 10° [1].

Thus, as j_z can be expressed in terms of u_Z and the ion mass density (ρ) as

$$j_z=\frac{Z_\mathrm{i}e}{m_\mathrm{i}}\rho(r,z)u_z(z) \tag{4}$$

from (2) we obtain

$$\rho(r,z)=\frac{m_\mathrm{i}I_\mathrm{i}}{Z_\mathrm{i}e\pi R^2(z)u_z(z)}\exp\left[-r^2/R^2(z)\right]. \tag{5}$$

Using also

$$j_r=\frac{Z_\mathrm{i}e}{m_\mathrm{i}}\rho(r,z)u_r(r,z) \tag{6}$$

we determine u_r as

$$u_r(r,z)=u_z(z)g(r,z) \tag{7}$$

where the function g is defined as

$$g(r,z)\equiv\frac{R(z)R'(z)}{r}\exp\left[r^2/R^2(z)\right]\times\left[2\left(1-\exp\left[-r^2/R^2(z)\right]\right)-r^2/R^2(z)\right]. \tag{8}$$

The θ component of the ion-momentum conservation equation is

$$u_r\frac{\partial u_\theta}{\partial r}+u_z\frac{\partial u_\theta}{\partial z}+\frac{u_ru_\theta}{r}=\frac{j_zB_r}{\rho}-\frac{j_rB_z}{\rho} \tag{9}$$

where u_θ is the azimuthal ion velocity and B_r and B_z are the radial and axial magnetic field components, respectively.

If in (9) the expressions for j_z, j_r, ρ, u_z, and u_r, from (2), (3), (5), and (7) are used, and one expresses u_θ as $u_\theta(r,z)=\Omega(z)r$, the following equation for $\Omega(z)$ is readily obtained:

$$r\frac{d\Omega}{dz}+2g\Omega=\frac{Z_\mathrm{i}e}{m_\mathrm{i}}(B_r-gB_z). \tag{10}$$

The equation $\nabla\cdot\mathbf{B}=0$ allows to express B_r, in the axially symmetric case considered, as

$$B_r=-\frac{1}{r}\int_0^r r'\frac{\partial B_z(r',z)}{\partial z}dr'.$$

With the approximation

$$\frac{\partial B_z(r',z)}{\partial z}\approx\frac{\partial B_z(0,z)}{\partial z}$$

$B_r(r,z)$ can be expressed as

$$B_r(r,z)\approx-\frac{r}{2}\frac{\partial B_z(0,z)}{\partial z}. \tag{11}$$

Using the analytical solution for the magnetic field of a finite solenoid we have checked that the approximation (11) is quite good in all regions of interest, resulting in differences below 10% or even close to the cathode and at radii close to the filter radius.

Besides, the Taylor r expansion of g is

$$g(r,z)=\frac{rR'(z)}{R(z)}\left[1-\frac{r^4}{6\,R^4(z)}-\frac{r^6}{12\,R^6(z)}+O\left(\frac{r^8}{R^8(z)}\right)\right]$$

which indicates that in the region where most of the plasma concentrates, $r<R(z)$, one can safely write $g(r,z)=rR'(z)/R(z)$. With this expression and (11), (10) can be written as

$$\frac{d\Omega}{dz}+\frac{2R'(z)}{R(z)}\Omega(z)=-\frac{Z_\mathrm{i}e}{2m_\mathrm{i}}\left(\frac{dB_z(0,z)}{dz}+\frac{2R'(z)}{R(z)}B_z(0,z)\right)$$

whose general solution is

$$\Omega(z)=-\frac{Z_\mathrm{i}eB_z(0,z)}{2m_\mathrm{i}}+\frac{C}{R^2(z)} \tag{12}$$

where C is a constant.

We consider now the axial and radial ion flow. The corresponding momentum equations can be written, with the

assumed expressions for the ion velocity, as

$$m_{\rm i}u_z\frac{\partial u_z}{\partial z} = -T_{\rm i}\frac{\partial}{\partial z}\ln(n_{\rm i}) + Z_{\rm i}e(E_z - u_\theta B_r) \quad (13)$$

$$m_{\rm i}\left(u_r\frac{\partial u_r}{\partial r} + u_z\frac{\partial u_r}{\partial z} - \frac{u_\theta^2}{r}\right) = -T_{\rm i}\frac{\partial}{\partial r}\ln(n_{\rm i}) + Z_{\rm i}e(E_r + u_\theta B_z) \quad (14)$$

where $n_{\rm i}$ is the ion density and the ion temperature $T_{\rm i}$ is assumed constant. By dividing (13) by $2K_{\rm i}$ (twice the ion kinetic energy), this equation can be written in the form

$$\frac{1}{u_z}\frac{\partial u_z}{\partial z} = -\frac{T_{\rm i}}{2K_{\rm i}}\frac{\partial}{\partial z}\ln(n_{\rm i}) - \frac{Z_{\rm i}e}{2K_{\rm i}}\frac{\partial\phi}{\partial z} - \frac{Z_{\rm i}eu_\theta B_r}{2K_{\rm i}}$$

where ϕ is the electrostatic potential. The ion kinetic energy $K_{\rm i}$ is about 50 eV, and $T_{\rm i} \approx 0.3$ eV [11]. Therefore, the ion flow is highly supersonic (Mach number $M \approx 12$) and one should expect a change of the axial flow velocity as the jet section changes. However, because the density and the velocity are related by mass conservation, their characteristic lengths of variation are similar, and so the pressure term (the first one in the right-hand side), responsible for the mentioned effect is smaller by about M^{-2} than the left-hand side. Moreover, ϕ is found to vary by only a few volts along the filter (see Fig. 4), so that the second term in the right-hand side is also small compared to the left-hand side. Finally, the last term can be estimated using $u_\theta(r,z) = \Omega(z)r$, with characteristics values $\Omega \approx 10^5$ s^{-1}, and $r \approx R \approx 10^{-2}$ m, [6] resulting to be smaller than 0.5 m^{-1}. From all this, the length scale for the variation of u_z can be evaluated to be well above the filter length, so that u_z can be assumed constant in the model.

On the other hand, as $n_{\rm i} = \rho/m_{\rm i}$, using (5) and (7), we can write from (14)

$$m_{\rm i}\left(\frac{u_z^2R''}{R} - \Omega^2\right) = \frac{2T_{\rm i}}{R^2} + Z_{\rm i}e\left(\frac{E_r}{r} + \Omega B_z\right) \quad (15)$$

where, as before, the approximation made is to neglect terms of order $(r/R)^3$ and higher in the left-hand side of (14), and to replace $u_\theta(r,z) = \Omega(z)r$. Again considering the smooth variations of B_z with r, as was done in (11) (or also from *a posteriori* estimations that allow to neglect the magnetic force compared to the electric force), the only term in (15) with an r dependence is E_r/r, and so E_r must be linear in r. Then writing $E_r = -\partial V/\partial r$, the electrostatic potential V is a quadratic function of r. As $\partial V/\partial r|_{r=0} = 0$, one can write

$$V(r,z) = V_0(z) + F(z)r^2 \quad (16)$$

where $F(z)$ is a function of z only, to be determined experimentally. Expression (16) allows to rewrite (15) as

$$\frac{m_{\rm i}u_z^2(z)R''(z)}{R(z)} = m_{\rm i}\Omega(z)^2 + \frac{2T_{\rm i}}{R^2(z)} + Z_{\rm i}e\left[\Omega(z)B_z(0,z) - 2\,F(z)\right]. \quad (17)$$

For strong enough values of the magnetic field, the magnitudes of the plasma reach almost z-independent profiles in the so called "equilibrium region" inside the filter (this z-independence is the definition of this region, in which also the magnetic field is almost uniform and is close to its maximum value, $B_z(r,z) = B_{\max}$). In this region, $R'' = 0$, $R = R_{\rm eq}$, and $F = F_{\rm eq}$, so, from (17), one has a relation among equilibrium values that allows the constant C in (12) to be determined. The result is

$$C = \left(\Omega_{\rm eq} + \frac{Z_{\rm i}eB_{\max}}{2m_{\rm i}}\right)R_{\rm eq}^2 \quad (18)$$

where

$$\Omega_{\rm eq} = -\frac{\Omega_{\rm ci}}{2}\left[1 \pm \sqrt{1 + \frac{8}{\Omega_{\rm ci}B_{\max}}\left(F_{\rm eq} - \frac{T_{\rm i}}{Z_{\rm i}eR_{\rm eq}^2}\right)}\right] \quad (19)$$

and $\Omega_{\rm ci}$ is the ion cyclotron frequency corresponding to $B_{\max}$

$$\Omega_{\rm ci} = \frac{Z_{\rm i}eB_{\max}}{m_{\rm i}}.$$

This expression is similar to the rigid rotor solution of Davidson [10]. The term proportional to $T_{\rm i}$ is related to the pressure term (diamagnetic term in Davidson´s expression), the term proportional to $F_{\rm eq}$ arises from the radial electric force ($\boldsymbol{E}$ cross $\boldsymbol{B}$ drift term in [10]). In this way, from measured values of $F_{\rm eq}$ and $R_{\rm eq}$, (12) completely determines the plasma angular velocity $\Omega(z)$ in terms of the plasma radius $R(z)$.

V. Interpretation of the Results

Experimentally, the values of $R(z)$ can be determined as in [6], fitting the measured current density, at each z position, with a Gaussian radial profile. On the other hand, $F(z)$ is determined using the voltage difference between probes three and one as

$$F(z) = \frac{V_{\rm pf}^3 - V_{\rm pf}^1}{(\Delta r_{3-1})^2}$$

where Δr_{3-1} is the distance between the two probes.

To proceed, it is worth noting that, according to the measured values, expressions (17) and (19) can be significantly simplified. In the first place, in (19), the relative importance of the different terms inside the radical is given as, for the radial electric field and the pressure terms

$$F_{\rm eq} : \frac{T_{\rm i}}{Z_{\rm i}eR_{\rm eq}^2} = \frac{Z_{\rm i}e\Delta V_{\rm eq}}{T_{\rm i}} : 1$$

where $\Delta V_{\rm eq} \equiv F_{\rm eq}R_{\rm eq}^2$. Considering that $\Delta V_{\rm eq}$ is about a few volts, and $T_{\rm i} \approx 0.3$ eV [11], the pressure term can be neglected.

For the remaining radial electric field term

$$\frac{8F_{\rm eq}}{\Omega_{\rm ci}B_{\max}} = \frac{8Z_{\rm i}e\Delta V_{\rm eq}}{m_{\rm i}(\Omega_{\rm ci}R_{\rm eq})^2}$$

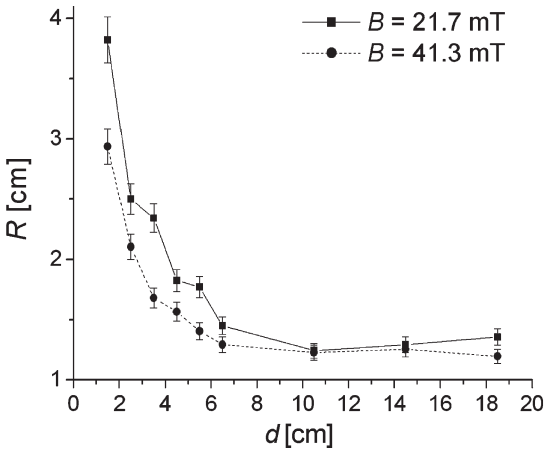

Fig. 6. Radial spatial scale of the Gaussian-density decay as a function of d for the two investigated B values. The lines are only a guide for the eye.

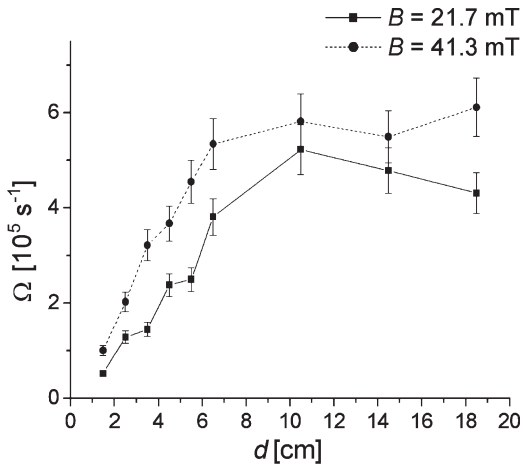

Fig. 7. Experimentally determined values of $\Omega(z)$ for $B = 21.7$ mT and $B = 41.3$ mT. The lines are only a guide for the eye.

since even for the highest magnetic field this relation turns out to be about 80, (19) can be approximately written as

$$\Omega_{\rm eq} = \pm\sqrt{\frac{2F_{\rm eq}\Omega_{\rm ci}}{B_{\max}}} = \pm\sqrt{\frac{2Z_{\rm i}eF_{\rm eq}}{m_{\rm i}}}. \qquad (20)$$

In a similar manner, the pressure and magnetic force terms in (17) can be neglected (compared to the radial electric field term) all along the duct because as one moves toward the filter entrance the electric term is even more important as the magnetic field and the plasma rotation decrease. On the other hand, the electric field does not change appreciably (this is later verified at the end of this section). In this way, (17) can be rewritten as

$$u_z^2(z)R''(z) = \Omega(z)^2R(z) - 2Z_{\rm i}eF(z)R(z)/m_{\rm i} \qquad (21)$$

where, to make the interpretation easy, (17) was multiplied by $R(z)$ and divided by $m_{\rm i}$, so that the first term in the right-hand side of (21) is (minus) the centripetal acceleration $(a_{\rm cp})$ of an ion at $r = R(z)$, and the second term is the corresponding radial electric force (per unit mass) that points in the $-r$-direction, while the left-hand side is the radial acceleration of the plasma column $(a_{\rm R})$. This expression, together with (12), is very helpful to understand the plasma behavior in terms of the experimentally determined values of $F(z)$ and $R(z)$.

In Figs. 6 and 7, the experimentally determined values of $R(z)$ and $\Omega(z)$, the latter given by (12), are respectively shown for $B = 21.7$ mT and $B = 41.3$ mT. It can be seen from Fig. 6 that the radius of the plasma column decreases as the plasma enters the filter until it approaches the equilibrium value after about 6 cm from the cathode. As one would expect, the column radii are smaller the higher the magnetic field is. The generation of rotation by the magnetic force is apparent in Fig. 7, reaching an equilibrium rotation value in the same duct region where the plasma radius did. Also, the rotational velocity is consistently higher for the higher magnetic field. It is worth noting that the constant in (12) was chosen from equilibrium values obtained well inside the filter, and not imposing zero rotation outside the filter.

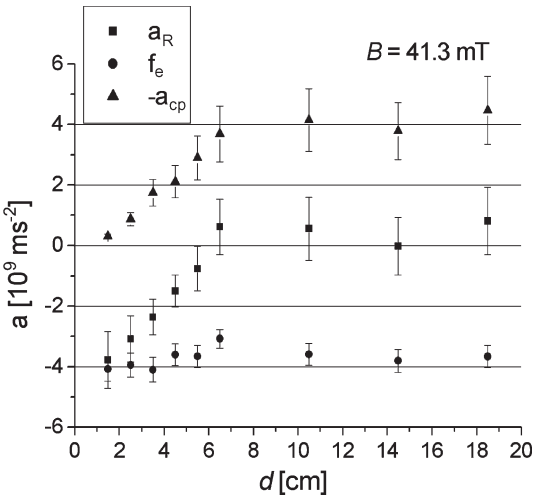

Fig. 8. Comparison of the different terms in the radial ion momentum (21) for $B = 41.3$ mT. $-a_{\rm cp}$ is proportional to minus the centripetal acceleration of an ion located at $r = R(z)$, $f_{\rm e}$ represents minus the electric force (per unit mass) on that ion and $a_{\rm R}$ represents the radial acceleration (per unit mass) of the ion.

In Fig. 8, the values of each of the terms in the right-hand side of (21) obtained from the experimentally determined values of $R(z)$ and $F(z)$, are shown as functions of d, for $B = 41.3$ mT. One of them $(-a_{\rm cp})$ is proportional to minus the centripetal acceleration of an ion located at $r = R(z)$, while the second $(f_{\rm e})$ represents minus the electric force (per unit mass) on that ion. For comparative purposes, the left-hand side term of the same equation $(a_{\rm R})$ has also been represented. $a_{\rm R}$ represents the radial acceleration (per unit mass) of the ion. The values of this last magnitude are those obtained from (21) as the difference between the two terms in its left-hand side, since the second spatial derivative cannot be calculated with enough precision from the experimentally determined values of $R(z)$. It is seen that $f_{\rm e}$ takes an almost constant value along the filter, while $-a_{\rm cp}$ is gradually increased up to its equilibrium value after $\sim$6 cm from the cathode. Note that in the equilibrium zone the derived plasma column acceleration is practically zero, consistent with a measured constant radius. A completely similar behavior is seen in the case $B = 21.7$ mT.

VI. Final Remarks

From the measurements and theory presented above, one can obtain the following picture of the plasma dynamics. As the plasma approaches the filter, a rotational motion is gradually generated by the magnetic force. In contrast, the radial electric force is already present and, quite remarkably, of a rather constant magnitude at the plasma edge $r = R(z)$ (remember that $R(z)$ changes appreciably with z). The radial acceleration of the plasma column is thus generated by this unbalance until enough rotation is generated to achieve equilibrium with $R(z) = \text{const}$. This equilibrium is of the rigid rotor type as was discussed in [6].

The plasma behavior is similar for the two investigated B values, for which the electrons are strongly magnetized while the ions are not. In both cases, the plasma reaches its equilibrium values at practically the same distance from the cathode. When comparing these equilibrium values for the cases with $B = 21.7$ mT and $B = 41.3$ mT, it can be seen that for the higher magnetic field, the angular velocity is about 15% bigger and the radius about 5% smaller. The electric field at the plasma equilibrium radius is about 10^3 V/m for $B = 21.7$ mT and 1.2×10^3 V/m for $B = 41.3$ mT. Even though these variations were in the expected direction, in the sense that a higher magnetic field leads to a more confined plasma, it is not worth for practical applications to double the magnetic field to obtain only a 5% reduction in the radius, which could be desirable to reduce the losses to the filter wall and/or to have a better ratio of the plasma to microdroplets. Another point to mention is that supersonic (high energy) ions that enter the filter are not slowed down along the filter, and so the filter does not affect the compactness of the coating. It can be seen in [6, Fig. 9] that for B values between 20 and 45 mT, R_{eq} does not present a significant variation. For magnetic fields below this range, not enough rotation is generated and the radial electric field is too small to produce confinement. Due to technical limitations, in this paper, magnetic fields higher than 45 mT were not investigated but it appears that little modifications in the quoted picture would appear at least for B values below the levels required to magnetize the ions.

References

[1] R. Boxman, D. Sanders, and P. Martín, *Handbook of Vacuum Arc Science and Technology, Fundamentals and Applications*. Park Ridge, NJ: Noyes, 1995.

[2] B. Cluggish, "Transport of a cathodic arc plasma in a straight, magnetized duct," *IEEE Trans. Plasma Sci.*, vol. 26, no. 6, pp. 1645–1652, Dec. 1998.

[3] J. Storer, J. Galvin, and I. Brown, "Transport of vacuum arc plasma through straight and curved magnetic ducts," *J. Appl. Phys.*, vol. 66, no. 11, pp. 5245–5250, Dec. 1989.

[4] D. B. Boercker, D. Sanders, J. Storer, and S. Falabella, "Modeling plasma flow in straight and curved solenoids," *J. Appl. Phys.*, vol. 69, no. 1, pp. 115–120, Jan. 1991.

[5] A. Anders, S. Anders, and I. G. Brown, "Transport of vacuum arc plasmas through magnetic macroparticle filters," *Plasma Sources Sci. Technol.*, vol. 4, no. 1, pp. 1–12, Feb. 1995.

[6] L. Giuliani, D. Grondona, H. Kelly, and F. Minotti, "On the plasma rotation in a straight magnetized filter of a pulsed vacuum arc," *J. Phys. D, Appl. Phys.*, vol. 40, no. 2, pp. 401–408, Jan. 2007.

[7] H Kelly, L Giuliani, and F Rausch, "Characterization of the ion emission in a pulsed vacuum arc with an axial magnetic field," *J. Phys. D, Appl. Phys.*, vol. 36, no. 16, pp. 1980–1986, Aug. 2003.

[8] B Koch, W Bohmeyer, and G Fussmann, "Angular dependency of the floating potential in a magnetized plasma," *J. Nucl. Mater.*, vol. 313–316, pp. 1114–1118, 2003.

[9] S. H. Lam, "Unified theory for the Langmuir probe in a collisionless plasma," *Phys. Fluids*, vol. 8, no. 1, pp. 73–87, Jan. 1965.

[10] R. C. Davidson, "Vlasov equilibrium and nonlocal stability properties of an inhomogeneous plasma column," *Phys. Fluids*, vol. 19, no. 8, pp. 1189–1202, Aug. 1976.

[11] F. Minotti, H. Kelly, and A. Lepone, "Two-dimensional fluid model for the interelectrode region of a non-filtered vacuum arc," *Plasma Sources Sci. Technol.*, vol. 11, no. 3, pp. 294–300, Mar. 2002.

Leandro Giuliani was born in Buenos Aires, Argentina, on November 26, 1974. He received the Master's degree in physics, with a thesis on plasma transport along a magnetic filter, from the Universidad de Buenos Aires, Buenos Aires, in 2005. He is currently working toward the Ph.D. degree in the Instituto de Física del Plasma, Consejo Nacional de Investigaciones Científicas y Técnicas (CONICET)-Facultad de Ciencias Exactas y Naturales, Universidad de Buenos Aires, under a fellowship from CONICET

Fernando Minotti was born in Buenos Aires, Argentina, on January 27, 1960. He received the Bachelor's degree in physics and the Ph.D. degree from the Universidad de Buenos Aires, Buenos Aires, in 1984 and 1990, respectively.

From 1991 to 1993, he held a postdoctoral position with the Goddard Institute for Space Studies, National Aeronautics and Space Administration, NY. Since 1993, he has been a Researcher with the Instituto de Física del Plasma, Consejo Nacional de Investigaciones Científicas y Técnicas (CONICET)-Facultad de Ciencias Exactas y Naturales, Universidad de Buenos Aires. Since 1998, he has been a Professor with the Universidad de Buenos Aires.

Diana Grondona was born in Buenos Aires, Argentina, on July 23, 1964. She received the M.S. and Ph.D. degrees in physics from the Universidad de Buenos Aires, Buenos Aires, in 1989 and 1994, respectively.

Since 1987, she has been with the Instituto de Física del Plasma, Consejo Nacional de Investigaciones Científicas y Técnicas (CONICET)-Facultad de Ciencias Exactas y Naturales, Universidad de Buenos Aires, where she is currently a CONICET Researcher. Her research interests include vacuum arcs and nonthermal high-pressure plasmas.

Héctor Kelly was born in Mendoza, Argentina, on February 14, 1948. He received the M.S. degree and the Ph.D. degree in physics from the Universidad de Buenos Aires, Buenos Aires, Argentina, in 1972 and 1979, respectively.

Since 1973, he has been a Researcher with the Instituto de Física del Plasma, Consejo Nacional de Investigaciones Científicas y Técnicas (CONICET)-Facultad de Ciencias Exactas y Naturales, Universidad de Buenos Aires. His research interests include high-power electric discharges and nonthermal high-pressure plasmas.